Hindawi
Journal of Computer Networks and Communications
Volume 2021, Article ID 4124230, 7 pages
https://doi.org/10.1155/2021/4124230

Research Article

SWIPT-Based Nonorthogonal Multiple Access under Arbitrary Nakagami-*m* Fading with Direct Links

Thanh-Luan Nguyen,[1] **Duy-Hung Ha**,[2] **Phu Tran Tin**,[1] **and Nguyen Van Vinh**[3]

[1]*Faculty of Electronics Technology, Industrial University of Ho Chi Minh City (IUH), Ho Chi Minh, Vietnam*
[2]*Wireless Communications Research Group, Faculty of Electrical and Electronics Engineering, Ton Duc Thang University, Ho Chi Minh, Vietnam*
[3]*FPT University, Hanoi, Vietnam*

Correspondence should be addressed to Duy-Hung Ha; haduyhung@tdtu.edu.vn

Received 8 April 2021; Revised 20 October 2021; Accepted 10 November 2021; Published 3 December 2021

Academic Editor: Giovanni Pau

This paper studies the joint impact of simultaneous wireless information and power transfer (SWIPT) and nonorthogonal multiple access (NOMA) to the cooperative relay (CoR) network where direct links exist. Over Nakagami-*m* fading environments, the near users employ decode-and-forward (DF) and energy harvesting (EH) to assist the transmission from the source to the far users. Exploiting the time-switching protocol (TSP) and power-splitting protocol (PSP) to the CoR-based NOMA system, analytical results for the outage probability are derived, and the corresponding throughput is obtained. Comparative results show that the PSP outperforms the TSP at low transmit power, while at high-transmit-power regime, the TSP provides similar performance as the PSP.

1. Introduction

Nonorthogonal multiple access (NOMA) has been recognized as a promising solution for spectral efficiency in wireless networks [1–8]. NOMA technology allows multiple access (MA) in the power domain and efficiently utilizes the spectrum by exploiting users' channel state information [7]. In [8], the authors study the performance of multihop NOMA systems under imperfect channel state information settings, and the results show that implementing NOMA provides a significant boost in the system performance.

In addition to NOMA, which provides high spectral efficiency, improving energy efficiency in future networks is also another major issue. One prominent approach is to apply simultaneous wireless information and power transfer (SWIPT) [9] to exploit incoming radio frequency signals for regenerative systems. Particularly, two practical protocols, namely, the time-switching-based protocol (TSP) and power-splitting-based protocol (PSP), are introduced for harvesting energy from wireless signals [10]. Furthermore, a decode-and-forward (DF) relaying system is implemented, in which some users utilize energy harvesting (EH) mechanisms to assist other users [11] with worse performance. Hybrid EH models for the TSP and PSP are also well studied in [12,13] in which energy harvesting offers a performance boost for OMA systems. In these works, the application of NOMA in cooperative networks is not considered. Although the authors in [14] present both NOMA and SWIPT, the PSP is favored for performance improvement while neglecting the TSP.

In [15, 16], only Rayleigh fading is considered which cannot model the potential LoS components and the TSP is not considered. Without direct links from the source nodes, the work in [17, 18] investigates a relay-assisted SWIPT-NOMA to serve multiple far users over simplified Nakagami-*m* channels with integer shapes. Similarly, the authors in [19] use the simplified Nakagami-*m* fading with integer fading severity to study the system performance. In the aforementioned works, nonlinear EH models are not adopted. However, the results in [20–22] show that the linear

EH model can be applied for performance analysis while retaining mathematical tractability compared to the non-linear counterpart.

In this paper, unlike most works, generalized Nakagami-m fading is considered for the SWIPT-based NOMA where the shape factors take arbitrary values. Subsequently, one can adjust m to capture various line-of-sight and non-line-of-sight fading channels [23, 24]. Furthermore, the results can be considered as approximations for the emerging techniques, e.g., satellite-terrestrial communication [25], underwater acoustic communication [26], and reconfigurable intelligent surfaces. Particularly, for delay-sensitive applications, the outage probability (OP) and throughput given fixed transmission rates are studied. Analytical results for the aforementioned metrics, unlike many existing papers, are provided in compact closed forms.

The rest of this paper is organized as follows. In Section 2, we present the cooperative NOMA system and energy harvesting protocols. Performance analysis for the TSP and PSP is also presented in Section 2. Monte Carlo simulations are then presented in Section 3 to validate our analysis and provide practical insights. Finally, we conclude our paper in Section 4.

2. Materials and Methods

2.1. System Model. As presented in Figure 1, the cooperative NOMA system consists of a single source node (S) an EH-enabled relay user (U_1), which can perform both EH and relay-based operations, and a low link strength user (U_2). In practice, S can be a base station in cellular network while U_1 and U_2 can be cell-center and cell-center users, respectively. In this paper, all channels are assumed to be block-fading, in which the channel states remain unchanged during a specific transmission block but vary independently from one block to another, following the Nakagami-m fading model. In addition, we consider that U_1 is an energy-constraint user and requires EH operations to support the relay transmission from S to U_2 using the decode-and-forward (DF) strategy.

2.2. Time-Switching Protocol (TSP). In Figure 2(a), the TSP is adopted at the relay user U_1 over a certain of block time T, in which α, $\alpha \in [0, 1]$ specifies the proportion of block time for EH from the source signal. Then, $(1-\alpha)T$ block time is equally divided for direct transmission, i.e., $S \longrightarrow U_1, U_2$, and relay transmission, i.e., $U_1 \longrightarrow U_2$. Assuming that U_1 is a buffer-free user, all the harvested energy is utilized by this user to assist U_2.

$$P_1 = P_S \frac{|h_1|^2}{d_1^{\mu}} \frac{2\alpha\eta}{1-\alpha}, \tag{1}$$

where $\eta \in [0, 1]$ specifies the EH efficiency, varying upon the designed circuitry.

Subsequently, the source S transmits a superimposed signal $x = \sqrt{\rho_1 x_1} + \sqrt{\rho_2 x_2}$, in which x_1 and x_2 are the desired unit-energy signal for user U_1 and U_2, respectively, and ρ_i denotes the power allocation for U_i, where $0 \le \rho_1 \le \rho_2 \le 1$ and $\rho_1 + \rho_2 = 1$ according to the NOMA principle [1–6]. Accordingly, the received signal-to-interference-plus-noise ratio (SINR) at U_1 and U_2 to detect x_2 is given by

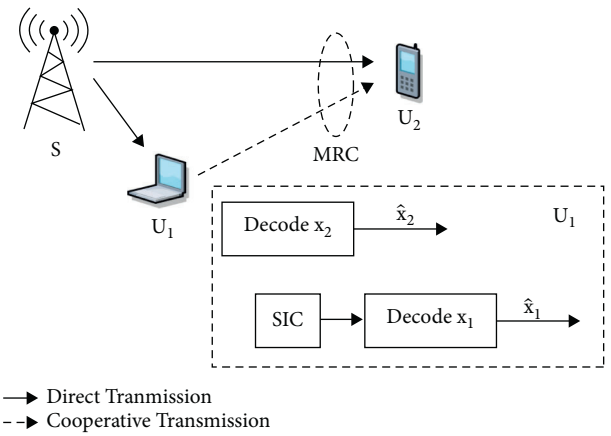

Figure 1: The SWIPT-based NOMA system.

$$\gamma_{2\longrightarrow 1} = \frac{\rho_2\beta_1}{\rho_1\beta_1 + 1}, \qquad \gamma_2 = \frac{\rho_2\beta_2}{\rho_1\beta_2 + 1}, \tag{2}$$

respectively, in which $\beta_1 = P_S|h_1|^2/d_1^{\mu}\sigma_1^2$ and $\beta_2 = P_S|h_2|^2/d_2^{\mu}\sigma_2^2$. At U_1, if the interference signal x_2 is correctly decoded, it then performs successive interference cancellation (SIC) to further detect its own information. Subsequently, the received signal-to-noise ratio (SNR) at U_1 to decode x_1 is

$$\gamma_1 = \rho_1\beta_1. \tag{3}$$

Subsequently, the U_1 forwards x_2 to U_2 in the cooperative phase. At U_2, maximal ratio combining (MRC) [8,14] is employed to obtain SNR as follows:

$$\gamma_2^{\mathrm{MRC}} = \gamma_2 + \beta_1\beta_0, \tag{4}$$

where $\beta_0 = (2\alpha\eta/1-\alpha)(|h_0|^2/d_0^{\mu}\sigma_2^2)$.

2.3. Power-Splitting Protocol (PSP). The PSP splits the received power received from the source S into a proportion of θP_S and $(1-\theta)P_S$, in which $\theta \in [0, 1]$ denotes the power-splitting ratio. The former proportion is utilized for EH, and the latter is for information processing at U_1. Similar to the TSP, the received SINRs at U_1 and U_2 for the PSP can be analogously obtained from those of the TSP by redefining β_1, β_2, and β_0 as $\beta_1 = (1-\theta)P_S|h_1|^2/d_1^{\mu}\sigma_1^2$, $\beta_2 = P_S|h_2|^2/d_2^{\mu}\sigma_2^2$, and $\beta_0 = (\theta\eta/1-\theta)(|h_0|^2/d_0^{\mu}\sigma_2^2)$, respectively.

2.4. Performance Analysis. In this section, the OP of SWIPT-aided cooperative NOMA networks with the TSP and PSP is presented. The motivation for examining the outage performance is two-fold. First, OP is defined as the probability for the received SINR/SNR at the receivers (U_1 and U_2) to fall below the rate threshold, which then can further be adapted

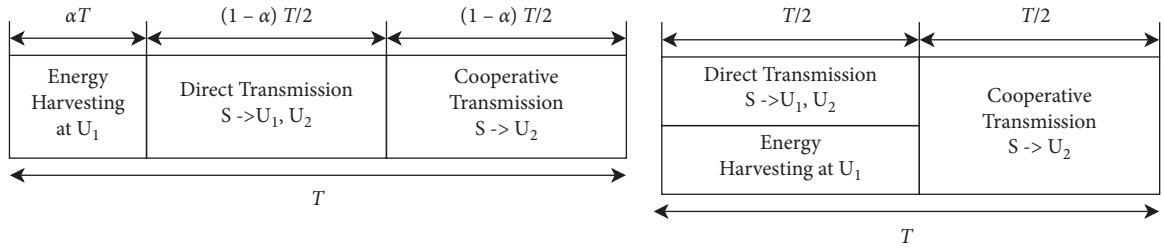

Figure 2: Block diagram for the transmission scheme for the (a) TSP and (b) PSP.

for examining the throughput in delay-sensitive networks. Furthermore, OP can be viewed as the performance bound for bit error rate (BER) analysis, another important performance metric, with an optimal coding scheme and infinite block length [23].

The OP at the U_2 is defined as the received SINR at this user falls below a decoding threshold, which guarantees the minimum quality-of-service (QoS) requirement for this user. In the proposed network, if the U_1 successfully decodes both x_2 and x_1, then it can assist the transmission from S to U_2 and the OP is defined via the received SNR from MRC receiver (γ_2^{MRC}); otherwise, it is defined via the received SINR during the first information transmission phase (γ_2). Mathematically speaking, the OP at U_2 is

$$\begin{aligned} OP_2 = {} & \Pr\left(\gamma_{2\longrightarrow 1} \geq \tau_2, \gamma_1 \geq \tau_1\right)\Pr\left(\gamma_2^{\mathrm{MRC}} < \tau_2\right) \\ & + \Pr\left(\gamma_{2\longrightarrow 1} < \tau_2 \text{ or } \gamma_1 < \tau_1\right)\Pr\left(\gamma_2 < \tau_2\right), \end{aligned} \tag{5}$$

where $\tau_i = 2^{2R_i/(1-\alpha)} - 1$ for the TSP and $\tau_i = 2^{2R_i} - 1$ for the PSP and R_i (bps/Hz) is the target rate for x_i, for $i = 1, 2$. Without loss of generality, let $\Omega_i = \mathbb{E}[\beta_i]$, where $\Omega_1 = P_S d_1^{-\mu}/\sigma_1^2$, $\Omega_2 = P_S d_2^{-\mu}/\sigma_2^2$ and $\Omega_0 = (2\alpha\eta/1-\alpha) d_0^{-\mu}/\sigma_2^2$ for the TSP and $\Omega_1 = (1-\theta) P_S d_1^{-\mu}/\sigma_1^2$, $\Omega_2 = P_S d_2^{-\mu}/\sigma_2^2$ and $\Omega_0 = (\eta\theta/1-\theta) d_0^{-\mu}/\sigma_2^2$ for the PSP. In addition, the CDFs and PDFs of β_i are modelled as

$$\begin{aligned} F_{\beta_i}(x) &= 1 - \frac{1}{\Gamma(m_i)}\Gamma\left(m_i, \frac{m_i}{\Omega_i}x\right), \quad x > 0, \\ f_{\beta_i}(x) &= \frac{1}{\Gamma(m_i)}\left(\frac{m_i}{\Omega_i}\right)^{m_i} x^{m_i - 1}\exp\left(-\frac{x m_i}{\Omega_i}\right), \quad x > 0, \end{aligned} \tag{6}$$

where $\Gamma(x)$ denotes the Gamma function [27] and $\Gamma(a, x) = \int_x^\infty t^{a-1}e^{-t}dt$ is the upper incomplete Gamma [27], equation (8.350.1). It is noted that the Nakagami-m distribution models consider line-of-sight components with m_i as an integer.

Theorem 1. *The OP at U_2 can be expressed in closed form as follows:*

$$\begin{aligned} OP_2 = {} & F\beta_1\left(\max\left(\frac{\tau_2}{\rho_2 - \tau_2\rho_1}, \frac{\tau_1}{\rho_1}\right)\right)F\beta_2\left(\frac{\tau_2}{\rho_2 - \tau_2\rho_1}\right) + \left(1 - F_{\beta_1}\left(\max\frac{\tau_2}{\rho_2 - \tau_2\rho_1}, \frac{\tau_1}{\rho_1}\right)\right) \\ & \sum_{k=1}^{K} F_{\beta_1\beta_2}\left(\frac{K-k+1}{K}\tau_2\right)\left(F_{\gamma_2}\left(\frac{k}{K}\tau_2\right) - F_{\gamma_2}\left(\frac{k-1}{K}\tau_2\right)\right). \end{aligned} \tag{7}$$

$\rho_2 > \tau_2\rho_1$, otherwise OP_2=1, K denotes the number of staircases representing the accuracy of the abovementioned analytical result, and

$$F_{\gamma_2}(x) = \begin{cases} F_{\beta_2}\left(\dfrac{\tau_2}{\rho_2 - \rho_1 x} \quad \dfrac{\rho_2}{\rho_1} > x\right), \\ 1, \qquad\qquad \text{otherwise}, \end{cases} \tag{8}$$

$$F_{\beta_1\beta_0}(\beta) = \frac{1}{\Gamma(m_0)\Gamma(m_1)} G_{1,3}^{2,1}\left(\frac{m_0 m_1}{\Omega_0\Omega_1}\beta\Big|_{m_0, m_1, 0}^{1}\right). \tag{9}$$

Proof. See Appendix. □

Remark 1. The introduced theorem can be applied over various fading channels since (7) and (8) are expressed directly via the CDF of β_1 and β_2. The main challenge is to derive that of $\beta_0\beta_1$. However, squared Nakagami-m distribution, i.e., Gamma distribution, is a Pareto type II distribution and can be adopted to fit various complex distributions. In other words, the theorem can be applied to study the performance of various networks such as Rician-shadowed [25] and $\kappa - \mu$-shadowed fading with the help of the work in [26].

Consequently, the throughput of x_2 for the network adopting the TSP and PSP is given by

$$T_2 = \frac{1-\alpha}{2}\left(1 - OP_2\right)\log_2\left(1+\tau_2\right), \quad T_2 = \frac{1}{2}\left(1 - OP_2\right)\log_2\left(1+\tau_2\right). \tag{10}$$

respectively.

2.5. Nonlinear Energy Harvesting. In the previous section, the linear EH model is adopted. In practice, the harvested power (P_1) is a nonlinear function of the input energy and is bounded by a certain threshold [22]. In order to capture this nonlinearity, one could replace the product $\beta_0\beta_1$ in (4) with $\widehat{\beta}_0\widehat{\beta}_1$ given by

$$\widehat{\beta}_0\widehat{\beta}_1 \triangleq \begin{cases} 0, & \psi\beta_1 < \overline{P}_{th}^{(1)}, \\ a_i\beta_1\beta_0 + b_i, & \overline{P}_{th}^{(i)} < \psi\beta_1 < \overline{P}_{th}^{(i+1)}, \quad i = 1, 2, \ldots, N-1, \\ \overline{P}_{\max}\dfrac{\beta_0}{\psi}, & \psi\beta_1 > \overline{P}_{th}^{(N)}, \end{cases} \tag{11}$$

where $\psi = 2\alpha\eta/1-\alpha$ for the TSP and $\psi = \theta\eta/1-\theta$ for the PSP, $\overline{P}_{\max} = P_{\max}/\sigma_1^2$ is the maximum output power normalized by noise, and $\overline{P}_{th}^{(i)} = P_{th}^{(i)}/\sigma_1^2$, a_i, and b_i are the normalized thresholds, the scopes, and the intercepts for the piecewise linear EH model in [22].

3. Results and Discussion

In this section, the derived analytical results are graphically presented to provide insights for the throughput at U_2. Let us assume equal noise power at each terminal $\sigma_2^2 = \sigma_1^2 = \sigma^2$ with density −133 dBm/Hz and a bandwidth of 10 MHz. In addition, the distances are set as $d_1 = 20\ m$, $d_0 = 60\ m$, and $d_2 = (d_1^2 + d_0^2)^{1/2}$, and the path loss exponent is set to 4. The fading severity factors are $m_1 = 2.2$, $m_0 = 1.4$, and $m_2 = 0.8$. The power allocations are $\rho_1 = 0.2$ and $\rho_2 = 0.8$, and the target data rates are $R_1 = 1.5$ bits/s/Hz and $R_2 = 0.5$ bits/s/Hz.

In Figure 3, the throughput at U_2 is presented as a function of EH ratios. As can be seen, the analytical result perfectly matches the simulation results which validates our analysis. As the EH ratio increases from zero, more resources (time or power) are spent on EH, and thus, the throughput at U_2 increases to its optimal values which are marked by blue stars in Figure 3. However, beyond this point, the throughput at U_2 then decreases as the resources for information processing at U_1 are gradually depleted which results in a higher outage at this user and prevents this user from assisting U_2. There exists a floor level which is the throughput obtained by the direct transmission. For the TSP, one can see it outperforms the PSP at low harvesting ratio values.

In Figure 4, the optimal throughput is obtained from an exhaustive search method by varying EH ratios with a step size of 0.001 and selecting the optimal values corresponding to a transmission power as discussed in Figure 3. It can be seen that, at high-transmit-power regimes, there exists a floor level where both the TSP and PSP provide similar optimal performance. In low-transmit-power regimes, the PSP performs better than the TSP, whereas they both have similar performance with higher transmit power, i.e., beyond 20 dBm. In addition, one can observe that the linear EH model provides a prominent bound for the nonlinear EH model where similar throughput can be observed at the high-transmission-power regime.

4. Conclusions

This paper studies the application of SWIPT to NOMA systems under Nakagami-m fading environments with arbitrary shapes. The analytical results of outage probabilities and system throughput are presented in tractable closed-form expressions which are then validated by Monte Carlo simulation. The TSP-based system requires fewer resources to obtain optimal performance compared to the PSP-based system. In terms of optimal throughput, the PSP outperforms the TSP in the low-transmit-power regime but provides similar throughput as the TSP in the high-transmit-power regime.

Appendix

Let us rewrite the OP as U_2:

$$\mathrm{OP}_2 = \underbrace{\Pr\left(\frac{\rho_2\beta_1}{\rho_1\beta_1+1} \geq \tau_2, \rho_1\beta_1 \geq \tau_1\right)}_{\Xi_1} \underbrace{\Pr\left(\gamma_2 + \beta_1\beta_0 < \tau_2\right)}_{\Xi_2} + \underbrace{\Pr\left(\frac{\rho_2\beta_1}{\rho_1\beta_1+1} < \tau_2 \text{ or } \rho_1\beta_1 < \tau_1\right)}_{\Xi_3} \underbrace{\Pr\left(\gamma_2 < \tau_2\right)}_{\Xi_4}. \tag{A.1}$$

The probability Ξ_1 can be further derived as

$$\Xi_1 = \Pr\left(\beta_1 \geq \frac{\tau_2}{\rho_2 - \tau_2\rho_1}, \beta_1 \geq \frac{\tau_1}{\rho_1}\right) = 1 - F_{\beta_1}\left(\max\left(\frac{\tau_2}{\rho_2 - \tau_2\rho_1}, \frac{\tau_1}{\rho_1}\right)\right), \quad \frac{\rho_2}{\rho_1} > \tau_2. \tag{A.2}$$

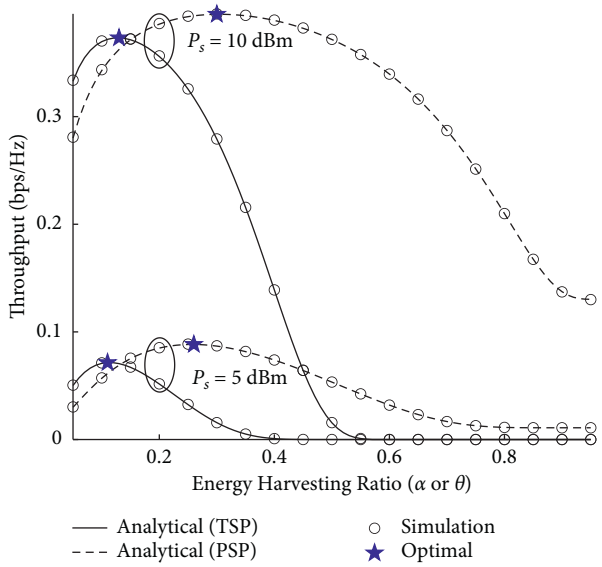

Figure 3: The throughput at U_2 versus the EH ratios and transmit power.

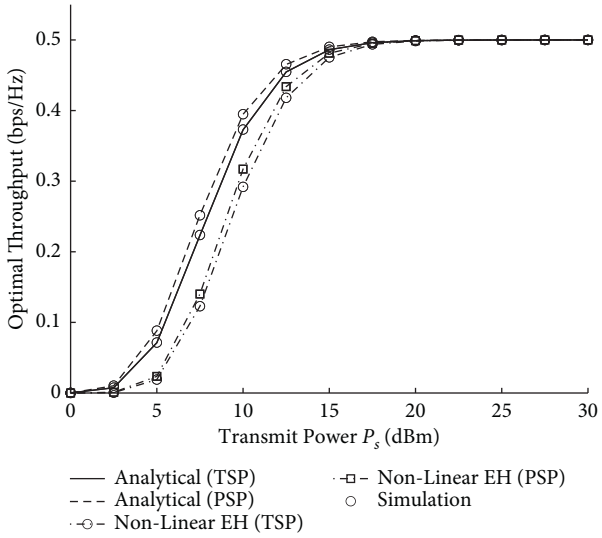

Figure 4: Optimal throughput versus the transmit power at the source node.

It can be noticed that $\Xi_3 = 1 - \Xi_1$; thus, we need to analyze the remaining probabilities Ξ_2 and Ξ_4. The second probability, Ξ_2, can be expressed via γ_2 and $\beta_1\beta_0$ as

$$\begin{aligned}\Xi_2 &= \int_0^{\tau_2} f_{\gamma_2}(x) \int_0^{\tau_2 - x} f_{\beta_1\beta_0}(y)\mathrm{d}y\mathrm{d}x,\\ &\overset{(a)}{=} \sum_{k=1}^{K} \int_{k-1/K\tau_2}^{k/K\tau_2} f_{\gamma_2}(x)\mathrm{d}x \int_0^{K-k+1/K\tau_2} f_{\beta_1\beta_0}(y)\mathrm{d}y,\\ &= \sum_{k=1}^{K} \left(F_{\gamma_2}\left(\frac{k}{K}\tau_2\right) - F_{\gamma_2}\left(\frac{k-1}{K}\tau_2\right)\right) F_{\beta_1\beta_0}\left(\frac{K-k+1}{K}\tau_2\right).\end{aligned} \tag{A.3}$$

In (A.3), $F_{\gamma_2}(x)$ and $F_{\beta_1\beta_0}(x)$ denote the CDF of γ_2 and $\beta_1\beta_0$, respectively, and (a) is obtained by using the K-step staircase approximation in [28]. First, the CDF $F_{\gamma_2}(x)$ can be derived straightforward as shown in Theorem 1. $\beta_1\beta_0$ is a product of two Gamma random variables β_0 and β_1 with shapes m_0 and m_1 and variances Ω_0 and Ω_1, respectively; thus, its CDF is given by [29]

$$F_{\beta_1\beta_0}(\beta) = \frac{1}{\Gamma(m_0)\Gamma(m_1)} G_{1,3}^{2,1}\left(\frac{m_0 m_1}{\Omega_0\Omega_1}\beta \middle| \begin{matrix} 1 \\ m_0, m_1, 0 \end{matrix}\right). \tag{A.4}$$

Finally, the last probability Ξ_4 is, by definition, the CDF of γ_2 measured at τ_2, i.e., $F_{\gamma_2}(\tau_2)$. By the foregoing results, the OP at U_2 can be obtained by Theorem 1.

Data Availability

No data were used to support this study.

Conflicts of Interest

The authors declare no conflicts of interest regarding the publication of this paper.

Authors' Contributions

T.-L. Nguyen and N. V. Vinh carried out the analysis and obtained numerical results. D.-H. Ha developed the system model and idea. P. T. Tin improved the majority of the writings.

Acknowledgments

This research was supported by Industrial University of Ho Chi Minh City (IUH) under grant no. 72/HD-DHCN.

References

[1] Y. Saito, A. Benjebbour, Y. Kishiyama, and T. Nakamura, "System-level performance evaluation of downlink non-orthogonal multiple access (NOMA)," in *Proceedings of the IEEE Annual Symposium on Personal, Indoor and Mobile Radio Communications (PIMRC)*, London, UK, September 2013.

[2] M. Vaezi, R. Schober, Z. Ding, and H. V. Poor, "Non-orthogonal multiple access: common myths and critical questions," *IEEE Wireless Communications*, vol. 26, no. 5, pp. 174–180, 2019.

[3] S. M. R. Islam, N. Avazov, O. A. Dobre, and K.-s. Kwak, "Power-domain non-orthogonal multiple access (NOMA) in 5G systems: potentials and challenges," *IEEE Communications Surveys & Tutorials*, vol. 19, no. 2, pp. 721–742, 2017.

[4] O. Maraqa, A. S. Rajasekaran, S. Al-Ahmadi, and H. Yanikomeroglu, "A survey of rate-optimal power domain NOMA with enabling technologies of future wireless networks," *IEEE Communications Surveys & Tutorials*, vol. 22, no. 4, pp. 2192–2235, 2020.

[5] J. Zeng, T. Lv, R. P. Liu, M. Peng, C. Wang, and J. Mei, "Investigation on evolving single-carrier NOMA into multi-carrier OMA in 5G," *IEEE Access*, vol. 6, pp. 48 268–48 288, 2018.

[6] B. Li, Z. Fei, and Y. Zhang, "UAV communications for 5G and beyond: recent advances and future trends," *IEEE Internet of Things Journal*, vol. 6, no. 2, pp. 2241–2263, 2019.

[7] Z. Ding, P. Fan, and H. V. Poor, "Impact of user pairing on 5G non-orthogonal multiple-access downlink transmissions," *IEEE Transactions on Vehicular Technology*, vol. 65, no. 8, pp. 6010–6023, 2016.

[8] P.-T. Tin, T.-T. Duy, and M. Voznak, "Security-reliability analysis of NOMA-based multi-hop relay networks in presence of an active eavesdropper with imperfect eavesdropping CSI," *Advances in Electrical and Electronic Engineering*, vol. 15, no. 4, pp. 591–597, 2017.

[9] L. R. Varshney, "Transporting information and energy simultaneously," in *Proceedings of the 2008 IEEE International Symposium on Information Theory (ISIT)*, Toronto, Canada, July 2008.

[10] A. A. Nasir, X. Zhou, S. Durrani, and R. A. Kennedy, "Relaying protocols for wireless energy harvesting and information processing," *IEEE Transactions on Wireless Communications*, vol. 12, no. 7, pp. 3622–3636, 2013.

[11] Y. Gu and S. Aïssa, "RF-based energy harvesting in decode-and-forward relaying systems: ergodic and outage capacities," *IEEE Transactions on Wireless Communications*, vol. 14, no. 11, pp. 6425–6434, 2015.

[12] T.-N. Nguyen, P.-T. Tin, D.-H. Ha et al., "Hybrid TSR–PSR alternate energy harvesting relay network over Rician fading channels: outage probability and SER analysis," *Sensors*, vol. 18, no. 11, Article ID 3839, 2018.

[13] P.-T. Tin, M. Tran, T.-N. Nguyen, and N.-T. Long, "System performance analysis of hybrid time power switching protocol of EH bidirectional relaying network in amplify-and-forward mode," *Indonesian Journal of Electrical Engineering and Computer Science*, vol. 14, no. No.1, pp. 118–126, 2019.

[14] Y. Liu, Z. Ding, M. Elkashlan, and H. V. Poor, "Cooperative non-orthogonal multiple access with simultaneous wireless information and power transfer," *IEEE Journal on Selected Areas in Communications*, vol. 34, no. 4, pp. 938–953, 2016.

[15] H. Q. Tran, C. V. Phan, and Q. T. Vien, "Performance analysis of power-splitting relaying protocol in swipt based cooperative NOMA systems," *EURASIP Journal on Wireless Communications and Networking*, vol. 110, 2021.

[16] Y. Ye, Y. Li, D. Wang, and G. Lu, "Power splitting protocol design for the cooperative NOMA with SWIPT," in *Proceedings of the 2017 IEEE International Conference on Communications (ICC)*, pp. 1–5, Paris, France, May 2017.

[17] X. Li, J. Li, Y. Liu, and A. Nallanathan, "Residual transceiver hardware impairments on cooperative NOMA networks," *IEEE Transactions on Wireless Communications*, vol. 19, no. 1, pp. 680–695, 2020.

[18] X. Li, J. Li, and L. Li, "Performance analysis of impaired SWIPT NOMA relaying networks over imperfect weibull channels," *IEEE Systems Journal*, vol. 14, no. 1, pp. 669–672, 2020.

[19] X. Li, Q. Wang, M. Liu, H. Peng, and J. Li, "Cooperative wireless-powered NOMA relaying for B5G IoT networks with hardware impairments and channel estimation errors," *IEEE Internet of Things J*, vol. 8, no. 7, pp. 5453–5467, 2021.

[20] Y. Liu, Y. Ye, H. Ding, F. Gao, and H. Yang, "Outage performance analysis for SWIPT-based incremental cooperative NOMA networks with non-linear harvester," *IEEE Communications Letters*, vol. 24, no. 2, pp. 287–291, 2020.

[21] X. Li, H. Mengyan, Y. Liu, V. G. Menon, A. Paul, and Z. Ding, "I/Q imbalance aware nonlinear wireless-powered relaying of B5G networks: security and reliability analysis," *IEEE*

Transactions on Network Science and Engineering (Early Access), 2020.

[22] L. Shi, W. Cheng, Y. Ye, H. Zhang, and R. Qingyang Hu, "Heterogeneous power-splitting based two-way DF relaying with non-linear energy harvesting," *IEEE GLOBECOM*, vol. 2018, pp. 1–7, 2018.

[23] D. N. C. Tse, P. Viswanath, and L. Zheng, "Diversity-multiplexing tradeoff in multiple-access channels," *IEEE Transactions on Information Theory*, vol. 50, pp. 1859–1874, 2004.

[24] M. K. Simon and M. Alouini, "Digital communications over fading channels," *IEEE Transactions on Information Theory*, vol. 54, no. 7, pp. 3369-3370, 2008.

[25] X. Yue, Y. Liu, Y. Yao, T. Li, X. Li, and R. Liu, "Outage behaviors of NOMA-based satellite network over shadowed-rician fading channels," *IEEE Transactions on Vehicular Technology*, vol. 69, no. 6, pp. 6818–6821, 2020.

[26] S. Kumar, "Approximate outage probability and capacity for $\kappa - \mu$ shadowed fading," *IEEE Wireless Communications Letters*, vol. 4, no. 3, pp. 301–304, 2015.

[27] I. S. Gradshteyn and I. M. Ryzhik, *Table of Integrals, Series, and Products*, AC Press, Inc., Cambridge, MA, USA, 4th edition, 1980.

[28] C. Zhang, J. Ge, J. Li, Y. Rui, and M. Guizani, "A unifed approach for calculating the outage performance of two-way AF relaying over fading channels," *IEEE Transactions on Vehicular Technology*, vol. 64, no. 3, pp. 1218–1229, 2015.

[29] K. Peppas, "Accurate closed-form approximations to Generalized-K sum distributions and applications in the performance analysis of equal-gain combining receivers," *IET Communications*, vol. 5, no. 7, pp. 982–989, 2011.